HHS Public Access

Author manuscript

J Cell Physiol. Author manuscript; available in PMC 2022 November 15.

Published in final edited form as:

J Cell Physiol. 2021 June ; 236(6): 4614–4624. doi:10.1002/jcp.30194.

Osteoblast-specific deficiency of ectonucleotide pyrophosphatase or phosphodiesterase-1 engenders insulin resistance in high-fat diet fed mice

Fiona L. Roberts[#1], **Nabil A. Rashdan**[#1], **Kanchan Phadwal**[1], **Greg R. Markby**[1], **Scott Dillon**[1], **Janna Zoll**[2], **Julian Berger**[3], **Elspeth Milne**[1], **Isabel R. Orriss**[4], **Gerard Karsenty**[3], **Olivier Le Saux**[2], **Nicholas M. Morton**[5], **Colin Farquharson**[1], **Vicky E. MacRae**[1]

[1]Functional Genetics and Development, The Royal (Dick) School of Veterinary Studies and The Roslin Institute, University of Edinburgh, Midlothian, UK

[2]Department of Cell and Molecular Biology, John A. Burns School of Medicine, University of Hawaii at Manoa, Honolulu, Hawaii, USA

[3]Department of Genetics and Development, Columbia University Medical Center, New York, New York, USA

[4]Department of Comparative Biomedical Sciences, The Royal Veterinary College, London, UK

[5]Centre for Cardiovascular Science, The Queen's Medical Research Institute, The College of Medicine and Veterinary Medicine, The University of Edinburgh, Edinburgh, UK

[#] These authors contributed equally to this work.

Abstract

Supraphysiological levels of the osteoblast-enriched mineralization regulator ectonucleotide pyrophosphatase or phosphodiesterase-1 (NPP1) is associated with type 2 diabetes mellitus. We determined the impact of osteoblast-specific Enpp1 ablation on skeletal structure and metabolic phenotype in mice. Female, but not male, 6-week-old mice lacking osteoblast NPP1 expression (osteoblast-specific knockout [KO]) exhibited increased femoral bone volume or total volume (17.50% vs. 11.67%; $p < .01$), and reduced trabecular spacing (0.187 vs. 0.157 mm; $p < .01$) compared with floxed (control) mice. Furthermore, an enhanced ability of isolated osteoblasts from the osteoblast-specific KO to calcify their matrix in vitro compared to *fl/fl* osteoblasts was observed ($p < .05$). Male osteoblast-specific KO and *fl/fl* mice showed comparable glucose and insulin tolerance despite increased levels of insulin–sensitizing undercarboxylated osteocalcin (195% increase; $p < .05$). However, following high-fat-diet challenge, osteoblast-specific KO mice

Correspondence: Kanchan Phadwal, Functional Genetics and Development, The Royal (Dick) School of Veterinary Studies and The Roslin Institute, University of Edinburgh, Easter Bush Campus, Midlothian EH25 9RG, UK. kanchan.phadwal@roslin.ed.ac.uk.

AUTHOR CONTRIBUTIONS

Conceived and designed the experiments: Fiona L Roberts, Nabil A Rashdan, Vicky E Macrae, Janna Zoll, Olivier Le Saux. Performed the experiments: Fiona L Roberts, Nabil A Rashdan, Greg R Markby, Scott Dillon, Julian Berger, Elspeth Milne, Isabel R Orriss. Analyzed the Data: Fiona L Roberts, Isabel R Orriss, Elspeth Milne. Manuscript preparation: Fiona L Roberts. Manuscript revision: Fiona L Roberts, Nabil A Rashdan, Greg R Markby, Scott Dillon, Kanchan Phadwal, Janna Zoll, Julian Berger, Elspeth Milne, Isabel R Orriss, Gerard Karsenty, Olivier Le Saux, Nicholas M Morton, Colin Farquharson, Vicky E MacRae.

SUPPORTING INFORMATION

Additional Supporting Information may be found online in the supporting information tab for this article.

showed impaired glucose and insulin tolerance compared with *fl/fl* mice. These data highlight a crucial local role for osteoblast NPP1 in skeletal development and a secondary metabolic impact that predominantly maintains insulin sensitivity.

Keywords

bone-fat interactions; genetic animal models; matrix mineralization; non-collagenous proteins; osteoblasts

1 | INTRODUCTION

Ecto-nucleotide pyrophosphatase or phosphodiesterase-1 ([ENPP1] in humans, ectonucleotide pyrophosphatase or phosphodiesterase-1 [NPP1] in mice) is the founding member of the ENPP family—which comprises of seven structurally related isozymes (Mackenzie et al., 2012; Roberts et al., 2019; Terkeltaub, 2006). Within bone, ENPP1 is highly expressed in the plasma membrane and mineral-depositing matrix vesicles of osteoblasts where its expression is over 30 times higher than in skeletal muscle (BioGPS, 2018; Roberts et al., 2019). ENPP1 is the principal generator of extracellular inorganic pyrophosphate (PP_i), a potent inhibitor of hydroxyapatite (HA) crystal formation in mineralization-competent tissues (Mackenzie et al., 2012). Mice lacking NPP1 (*Enpp1*$^{-/-}$) have severe hypermineralisation defects, which are associated with abnormally low plasma PP_i levels (Huesa et al., 2014; Li et al., 2013; Mackenzie et al., 2012). We, and others, have previously reported the dramatic effects of global *Enpp1* ablation on soft tissue calcification and hyperostosis of vertebrae and joints, highlighting ENPP1 as a critical regulator of mineralization through the production of PP_i (Anderson et al., 2005; Babij et al., 2009; Hajjawi et al., 2014; Harmey et al., 2004; Johnson et al., 2001; Johnson et al., 2003).

Surprisingly we, and others, have indicated *Enpp1*$^{-/-}$ mice have reduced trabecular bone mass and cortical thickness of both the tibia and femur (Li et al., 2013; Mackenzie et al., 2012). This reduction may be a consequence of relatively low levels of endogenous NPP1 expression throughout the long bones when compared to flat bones, such as calvaria (Anderson et al., 2005). For long bones, a complete ablation of NPP1 activity likely reduced extracellular PPi to abnormally low levels. Because of this, there is likely a reduced conversion of PPi to inorganic phosphate (Pi) by tissue specific alkaline phosphatase (TNAP). This TNAP-specific breakdown of PPi to Pi is critical for normal mineral formation and this process is likely disrupted in *Enpp1*$^{-/-}$ mice.

Further to the action in the control of mineralization, ENPP1 plays a recognized role in metabolic disease (Goldfine et al., 2008; Prudente et al., 2009). Indeed, our studies challenging *Enpp1*$^{-/-}$ mice with chronic exposure to a high-fat diet (HFD) revealed that global *Enpp1* gene deletion promotes improved glucose homeostasis in the context of obesity-associated diabetes (Huesa et al., 2014). Whilst the tissue origin of the metabolically active ENPP1 is presently unknown, it is possible that ENPP1 function may be directly controlled through the actions of osteoblast-derived hormonally active osteocalcin. Osteocalcin is bioactive when in the under- or uncarboxylated state and is known to have insulin sensitizing properties (Karsenty & Olson, 2016; Karsenty et al., 2012)

In the present study, we hypothesized that osteoblast-specific NPP1 ablation results in reduced mineralization of skeletal tissue and metabolic protection following chronic HFD feeding. To test this we generated mice with osteoblast-specific deletion of *Enpp1* to determine their skeletal development and structure as well as metabolic changes associated with insulin sensitivity and glucose homeostasis.

2.| MATERIALS AND METHODS

2.1 | Generation of osteoblast-specific *Enpp1* deficient mice

Floxed Enpp1 mice (*fl/fl*) were generated by Cyagen Biosciences. Osteocalcin-cre mice (*Ocn*-cre) were kindly donated by Thomas Clemens at John Hopkins Medicine, Baltimore, Maryland (Zhang et al., 2002). The commercially generated *fl/fl* mice were designed with the *loxP* sites around exon 9 (Figure S1a; Cyagen Biosciences). Mice were crossed to generate the osteoblast-specific conditional knockout mice (cKO) as well as appropriate *fl/fl* mice. Polymerase chain reaction (PCR)-based genotyping was performed on mouse DNA using a duplex PCR reaction for *Cre* (F:GCA TTA CCG GTC GAT GCA ACG AGT GAT GAG; R:GAG TGA ACG AAC CTG GTC GAA ATC AGT GCG) and *Fabpi200* (F:TGG ACA GGA CTG GAC CTC TGC TTT CCT AGA; R:TAG AGC TTT GCC ACA TCA CAG GTC ATT CAG) or *Enpp1* (F:GCTAATCATCAGGAGGTCAAG; R:CTGGTAGAATCCCGTCAATC). The specificity of the gene deletion was confirmed with western blot analysis of whole-bone tibial lysates (Figure S1b,c) with 85% efficiency of Cre recombinase activity. All mice were kept in polypropylene cages, with light/dark 12-hour cycles, at 21 ± 2°C. Mice for skeletal phenotyping (male and female mice) were fed ad libitum with control diet (6.2% fat; Harlan Laboratories) from 4 to 22 weeks of age. For metabolic phenotyping, only male mice were fed with a HFD (58% fat; Research Diets, Inc, New Brunswick) or control diet (6.2% fat; Harlan Laboratories) from 4 to 16 weeks of age. For metabolic phenotyping, ad libitum food consumption and weight gain were monitored throughout the experiments. Roslin Institute's Animal Users Committee approved all experimental protocols and the animals were maintained in accordance with UK Home Office guidelines for the care and use of laboratory animals.

2.2 | Glucose and insulin tolerance tests

Sixteen-week-old male mice were fasted for 4 h and administered 2 mg of $_D$-glucose (Sigma-Aldrich) per gram of body weight by oral gavage for glucose tolerance testing. For insulin tolerance testing, 16-week-old male mice were fasted for 4 h and administered 0.5 (control diet) or 0.75 (HFD) mU of insulin by intraperitoneal injection (Actrapid; NovoNordisk) per g of body weight. At 0, 15, 30, 60, and 120 min after insulin administration, blood glucose was measured with an Accu-Chek® Aviva glucose meter (Roche Diagnostics Ltd) and plasma insulin was measured by ELISA (ChrystalChem). Mice were allowed to recover for up to 1 week before being culled. Tissues, including pancreas, kidney, quadriceps femoris, femora, humerus and tibiae as well as brown, subcutaneous, mesenteric and gonadal fat pads, were collected and fixed for at least 24 h in 10% neutral-buffered formalin (NBF) for histological assessment and gene expression analysis.

2.3 | Plasma analysis

Immediately following euthanasia, blood was obtained from 6- and 16-week-old mice and plasma samples prepared. Blood was collected in eppendorfs coated with 2% ethylenediaminetetraacetic acid (EDTA) on ice. After centrifugation (10 min, 1000 *g*, 4°C), platelets were depleted from plasma by filtration (25 min, 2200 *g*, 4°C) through a Centrisart I 300,000 kD mass cutoff filter (Sartorius) and stored at −20°C until further processing. Total, carboxylated (GLA), undercarboxylated (GLU13-OCN) and uncarboxylated (GLU) osteocalcin was measured as previously described (Ferron et al., 2010), as well as markers of bone formation (P1NP; AmsBio) and resorption (CTx; AmsBio) and insulin, measured by ELISA (ChrystalChem). The plasma PP_i concentration was determined as described previously (Jansen et al., 2013).

2.4 | Microcomputed tomography and mechanical testing

Tibiae and femora from 6-week-old male and female mice were dissected and were immediately fixed in 10% NBF for 24 h and subsequently stored in 70% ethanol pending analysis. High-resolution scans with an isotropic voxel size of 4–5 μm were acquired with a microcomputed tomography system (μCT; 50 kV, 200 μA AI filter, 0.4° rotation step, Skyscan 1172, Bruker microCT) as previously described (Hajjawi et al., 2014). Scans were reconstructed using NRecon software (Brukker microCT). For each bone, a 1 mm section of the metaphysis was analyzed, using the base of the growth plate as a standard reference point. A 0.4 and 2.5 mm offset from the growth plate was used for trabecular and cortical bone, respectively. Data were analyzed with CtAn software (Bruker microCT). For calculation of bone mineral density, an appropriate calibration of the Skyscan CT analyzer was conducted using known density calcium HA phantoms scanned and reconstructed under identical conditions.

2.5 | Tissue histology

Dissected soft tissues were fixed in 4% paraformaldehyde (PFA) or 10% NBF (pH 7.4), processed using standard protocols using a Leica Arcadia tissue processor, and embedded in paraffin wax. Here, 4–8-μm sections (section thickness dependent on the stain used) were stained with haematoxylin and eosin (H&E) to assess tissue architecture and with Von Kossa or Alizarin Red-S to assess soft tissue calcification (Mackenzie et al., 2012). Liver sections were stained with picrosirius red (with fast-green counter stain) to assess fibrosis (Henderson et al., 2013). Adipocyte diameter and number, and pancreatic β-cell islet number and size were quantified using ImageJ software as previously described (Huesa et al., 2014; Rueden et al., 2017). Long bones (femora and tibia) were fixed, decalcified in 10% EDTA for 14 days at 4°C and embedded in wax. Subsequently, 4 μM sections were stained with H&E or toluidine blue. The femoral distal growth plate width was determined using Image J software (Rueden et al., 2017)

2.6 | Primary calvarial osteoblast cell culture

Primary calvarial osteoblasts were isolated from the calvariae of 3- to 5-day-old mice as previously described (Huesa et al., 2014). Cells were seeded at a density of 100,000 cells/well in six-well plates, in growth medium consisting of α-Minimum Essential Medium

(Invitrogen) supplemented with 10% fetal bovine serum (Invitrogen) and 1% gentamicin (Invitrogen). Mineralization was induced with the addition of 50 μg/ml ascorbic acid and 5 mM β-glycerophosphate as previously describe (Staines et al., 2017). In brief, cells were grown to confluence. Cells were maintained in a 5% CO_2 atmosphere at 37°C and the medium was changed every second or third day. Cells were either processed for RNA extraction or fixed in 4% PFA and stained with 2% Alizarin Red S (pH 4.2) for 5 min at room temperature. Alizarin Red S-stained cultures were extracted with 10% cetylpyridinium chloride for 10 min and optical density was measured at 570 nm. Calcium deposition was also quantified based on a method previously described (Zhu et al., 2013; Zhu et al., 2015). Briefly, cells were rinsed twice with phosphate-buffered saline and decalcified with 0.6 M HCl at room temperature for 2 h. Free calcium was determined colorimetrically by a stable interaction with phenolsulphonethalein, using a commercially available kit (Randox Laboratories Ltd.).

2.7 | Western blot analysis

The bone marrow of bones (humeri) was removed by centrifugation, and bones were homogenized in RIPA buffer (Sigma-Aldrich) with protease inhibitor cocktail (Sigma-Aldrich) using an IKA homogenizer (Sigma-Aldrich). Western blot analysis was conducted with specific antibodies against ENPP1 (Pierce) and β-actin (Abcam) and performed as previously described (Zhu et al., 2011; Zhu et al., 2013) and visualized using the enhanced chemiluminescence western blot analysis detection system (GE Healthcare).

2.8 | RNA extraction and quantitative polymerase chain reaction

RNA was isolated from bone (bone marrow removed), muscle and fat tissues using Qiazol (Qiagen) following standard protocol procedures. RNA from all other tissues and cell cultures were extracted with the RNeasy Qiagen kit following the manufacturers' instructions (Qiagen). RNA was quantified and reverse-transcribed as previously described (Zhu et al., 2011). All genes were analyzed with the SYBR green detection method (Roche) using the Stratagene Mx3000P real-time QPCR system (Agilent Technologies). All gene expression data were normalized against *β-actin*. All primers (*Tnap*, *Runx2*, *phospho1*, and *Ank*) were obtained from Qiagen, Sigma, and Primer Design (Primer Design).

2.9 | Statistics

Data are expressed as the mean ± *SEM* of at least three replicates per experiment. Standard comparisons between mice genotypes were analyzed by unpaired Student's *t* test. Comparisons between genotype and diet were analyzed with two-way analysis of variance (ANOVA). Time-course experiments were analyzed with a repeated-measures two-way ANOVA. Analysis was carried out using Minitab 16 (Minitab Ltd). A $p < .05$ was considered to be significant; *p* values of <.05, <.01, and <.001 were noted as *, **, and ***, respectively.

3 | RESULTS

3.1 | *Enpp1* deletion in osteoblasts results in increased trabecular bone mass in female mice

Comprehensive high-resolution μ-CT scanning revealed gender-dependent effects on tibial and femoral trabecular structural parameters, and less so in cortical bone. Examination of the mid-diaphyseal cortical bone of femora from 6-week-old female cKO mice showed increased femoral bone volume/total volume (17.50% vs. 11.67%; $p < .01$), endosteal diameter (1.95 vs. 1.67 mm; $p < .001$), and open porosity (2.46% vs. 2.04%; $p < .05$) compared to femora from female *fl/fl* mice (Table 1). Six-week-old female cKO also exhibit increased tibia endosteal diameter (1.48 vs. 1.29 mm; $p < .001$) compared to femora from female *fl/fl* mice (Table 1).

Male 6-week-old cKO mice demonstrate reduced cortical thickness (0.109 vs. 0.117 mm; $p < .05$) in the mid-diaphyseal femoral bone, and increased tibial periosteal diameter (1.817 vs. 1.660 mm; $p < .05$) compared to male *fl/fl* mice (Table 1). No differences in long bone trabecular parameters were observed for male mice (Table 2). In addition, female cKO mice showed decreased trabecular pattern factor (15.29 vs. 23.33; $p < .01$, Table 2; Figure S1d,e) in the trabecular compartment of the femur. The structure model index, which quantifies the architecture of a 3D structure in terms of amounts of plates and rods composing the structure (Hildebrand & Ruegsegger, 1997), was also significantly lower in femora from female cKO mice (1.39 vs. 1.66; $p < .01$, Table 2) compared to *fl/fl* mice. This indicates that the trabeculae in cKO mice appear to be more “plate-like” and more connected. Comparable changes were also observed in the tibia of cKO female mice. Interestingly, no differences in the bone-resorption marker CTx (Figure S1f) or the bone-formation marker P1NP (Figure S1f) were observed.

3.2 | Mice with osteoblast-specific ablation of *Enpp1 show* physiological plasma levels of the mineralization inhibitor PPi

We next addressed whether the cKO mice displayed depressed levels of PP_i, resembling that previously reported for *Enpp1*$^{-/-}$ mice (Terkeltaub, 2006). No notable differences in PP_i levels in male or female mice (Figure S1h) were observed. Subsequent alizarin red staining of metabolically - related soft tissues (e.g., pancreas) mineralization-related soft tissues (e.g. whisker follicle, aorta) and viscera tissues reveals an absence of pathological calcification (Figure S2a–j) in cKO mice when compared to *fl/fl* mice. Furthermore, absence of pathological calcification was also observed in femorotibial joint (Figure S2k,l).

3.3 | *Enpp1* deficient osteoblasts exhibit an enhanced ability to mineralize a matrix in vitro

To assess whether NPP1 plays a key role in osteoblast-mediated mineralization, we analyzed calcium deposition in 28-day cultured cKO osteoblasts, in comparison to *fl/fl* cells. Qualitative (Figure 1a) and quantitative (Figure 1b,c) analyses of calcium deposition indicated an enhanced ability of cKO osteoblasts to calcify their matrix. We also examined the messengerRNA (mRNA) expression of key osteogenic and mineralization associated genes in cKO osteoblasts. *Alpl*, *Runx2*, and *Phospho1* were all significantly increased in

cKO osteoblasts compared to *fl/fl* cells following culture until cellular monolayer confluence was reached (termed Day 0; $p < .05$; Figure 1d). No differences in the mRNA expression levels of the PP_i transporter *Ank* were noted (Figure 1d).

3.4 | Male mice with osteoblast-specific ablation of *Enpp1* show normal glucose tolerance and an elevated bioactive osteocalcin levels

We next tested whether the osteoblast-specific deletion of *Enpp1* also translates into changes in whole-body glucose metabolism in male mice. Sixteen-week-old male cKO and *fl/fl* male mice fed the control-diet showed similar glucose and insulin tolerance (Figure S3a–d). The size and number of pancreatic islets in control-diet fed cKO and *fl/fl* male mice were similar (Figure S3a,b). Additionally, there were no differences in fat pad mass (Figure S4d,e). Furthermore, no changes in mRNA expression levels of key genes for glucose transport (*Slc2a1*, *Slc2a4*, *Slc2a10*, *Slc2a12*) in gonadal fat were found (data not shown).

A significant increase in left and right *quadratus femoris* muscle mass from the control-diet fed cKO mice was observed when compared with *fl/fl* mice (left: 8.45 vs. 7.46 mg; $p < .05$, right: 8.48 vs 7.38 mg, $p < .05$; Figure 2a).

We recently published novel findings revealing that global $Enpp1^{-/-}$ mice have increased levels of the insulin-sensitizing bone-derived hormone osteocalcin (Huesa et al., 2014). The present study established that this observation may be specific to the actions of NPP1 in osetoblasts, with cKO mice also exhibiting significantly increased concentrations of undercarboxylated (GLU13) and osteocalcin (22.87 vs. 11.74 ng/ml; $p < .05$; Figure 2b) (Ferron et al., 2010). Total osteocalcin levels were comparable to *fl/fl* mice (Figure 2c).

3.5 | Male mice with osteoblast-specific ablation of *Enpp1* exhibit insulin resistance in response to chronic HFD challenge

We next investigated the effect of chronic high fat diet feeding on whole body glucose metabolism in 16-week-old male cKO mice. Following chronic HFD-challenge (12 weeks), no significant differences were observed between genotypes in body weight gain (Figure 3a), pancreatic islet morphology (Figure 3b,c) or white fat mass (Figure 3d) of male mice. However, cKO male mice showed a significant increase in brown fat mass (22.2%; $p < .05$; Figure 3d). Furthermore, the gonadal fat depot of the cKO male mice showed decreased average number of adipocytes per micrograph (85.19 vs. 283.19; $p < .001$; Figure 3e) and increased average adipocyte area (6215 vs. 3051.28 μm^2; $p < .01$; Figure 3f) compared to *fl/fl* male mice.

Impaired glucose tolerance ($p < .05$; Figures 4a,d) and reduced insulin sensitivity was observed in HFD challenged cKO male mice ($p < .05$; Figures 4b,d). However, no significant difference was observed between genotypes in glucose-stimulated insulin secretion (Figure 4c,d), indicative of relative preservation of normal β-cell function and peripheral insulin resistance in the male mice.

4 | DISCUSSION

The mineralization process depends on a regulated balance of various protein inducers and inhibitors. Indeed the application of mutant mouse models lacking NPP1 has highlighted the crucial role of NPP1 in regulating bone mineralization. However, these mice surprisingly show an osteopenic phenotype, despite the depressed levels of the circulating mineralization inhibitor PP_i (Mackenzie et al., 2012). Our present study reveals for the first time the precise role of osteoblastic NPP1 bone formation; with a specific ablation of NPP1 from osteoblasts increasing bone mass evidenced through bone volume fraction parameters. Indeed, a notable increase in bone volume or total volume was observed in female mice (Table 2). The lack of bone changes in the male compared to female mice may be underpinned by the different signaling pathways activated by the androgen and estrogen receptors within bone and warrants further investigation.

Calvarial osteoblasts lacking NPP1 showed increased mineralization potential in vitro, consistent with increased markers of osteogenic differentiation and mineralization. These novel data suggest that the local generation of PP_i from nucleotide precursors by NPP1 within the bone microenvironment directly regulates the ratio of P_i to PP_i, controlling the deposition of bone mineral. This ratio may be further modified by the upregulated *Alpl* expression observed in cKO osteoblasts, which may accelerate PP_i degradation and the simultaneous generation of P_i, thus promoting mineralization. Indeed ablating both NPP1 and TNAP function in mice has previously highlighted site-specific effects of NPP1, with normalization of the degree of mineralization seen in the joints, vertebrae and soft tissues, yet hypomineralisation of the long bones remaining (Millán, 2013). Relatively low levels of endogenous NPP1 expression in long bones compared to other tissues, reducing extracellular PP_i to abnormally low levels was proposed to underpin this phenotype. This study reveals that osteoblast specific NPP1 ablation is not sufficient to replicate the severe hypermineralisation of the connective tissues, including significant arterial calcification, observed in adult $Enpp1^{-/-}$ mice (Mackenzie et al., 2012). Additionally, these cKO mice do not show vertebrae hyperostosis or excessive bone production in the femorotibial joint, in contrast to $Enpp1^{-/-}$ mice. Together these results suggest that the circulatory PP_i generated from liver-derived NPP1 may be exerting crucial systemic protective effects against ectopic mineralization. Thus, the prevailing mechanistic hypothesis suggests that ATP-binding cassette C6 (ABCC6) mediates ATP release within the liver (R. S. Jansen et al., 2014). This ATP is subsequently hydrolyzed by hepatic ENPP1 to PP_i, which acts as an endocrine inhibitor of calcification at distant target sites. Indeed, ectopic mineralization and reduced circulating PP_i levels are observed in *Abcc6* deficient mice. Interestingly, $Abcc6^{-/-}$ which constitutively express human ENPP1 show increased plasma PP_i levels with small mineralization foci within connective tissues. This indicates an alternative mechanism, independent of PP_i, by which ABCC6 prevents ectopic mineralization (Zhao et al., 2017). This mechanism may work in tandem with CD73, an ecto-5′-nucleotidase that degrades AMP to adenosine and P_i (St Hilaire et al., 2011), to maintain low TNAP levels and prevent pathological mineralization (Ziegler et al., 2017). Further investigations examining the tissue specific contribution of NPP1 from liver will be key to elucidating the precise role of NPP1 in this multi-faceted pathway.

NPP1 negatively modulates insulin receptor signaling and has been proposed as a pathogenic factor predisposing to insulin resistance (Goldfine et al., 2008; Prudente et al., 2009). Indeed our laboratory has recently provided key evidence highlighting that NPP1 ablation protects against insulin resistance, obesity and diabetes (Huesa et al., 2014). Following the recent emergence of bone as an endocrine regulator, and given the fundamental importance of NPP1 in bone mineralization, it is essential to elucidate the contribution of osteoblastic NPP1 to the regulation of glucose metabolism. Intriguingly, we show here that osteoblast-specific NPP1 deficiency drives an unexpected worsening of insulin sensitivity relative to *fl/fl* mice chronically exposed to a HFD, despite elevated levels of the insulin-sensitizing form of osteocalcin.

Furthermore, these mice demonstrate white (gonadal, mesenteric, and sub-cutaneous depots) adipose tissue hypertrophy which is reported in the literature to be associated with metabolic impairment including insulin resistance (Kim et al., 2014). The cKO mice also present with a notable increase in brown adipose tissue mass of 22%. This is likely due to the mild thermogenic stress of room-temperature housing whereby the mice undergo alterations in non-shivering thermogenesis, which over time increases brown adipose tissue mass and activity (Feldmann et al., 2009; Lim et al., 2012; Nedergaard & Cannon, 2010; Xue et al., 2009). However, no significant differences in the mRNA levels of genes like solute carrier family 2 member 1 and 4 (*Slc2a1* and slc2a4), diacylglycerol O-acyltransferase 1 and 2 (*Dgat1* and *Dgat2*), uncoupling protein 1 and 2 (*Ucp1*, *Ucp2*), and lipoprotein lipase (*Lpl*) associated with thermogenic functionality were observed (Figure S5). The links between brown adipose tissue and bone are established, including positive correlation of brown adipose tissue volume and bone mineral density and bone cross sectional area (Bredella et al., 2012; Bredella et al., 2014; P. Lee et al., 2013). Our data suggests that osteoblast-specific NPP1 may be important in regulating bone and brown fat tissue homeostasis and subsequent brown adipose tissue activity. Additionally, the cKO mice present with increased *quadriceps femoris* muscle, yet do not present with metabolic protection. As such, it is likely that this *quadriceps femoris* muscle increase is not associated with the protective cardiometabolic effects observed in chronic caloric excess (e.g., obesity) as reported for increased appendicular skeletal mass in other mouse studies (Lee, Kim et al., 2019). These data suggest that the protection against diabetes reported in *Enpp1*$^{-/-}$ mice is likely due to the actions of nonskeletal NPP1 and indicate that NPP1 inhibition at one of its major sites of expression is metabolically detrimental. Interestingly, a differential sex-related sensitivity has been reported in obesity and insulin resistance-related cardiometabolic diseases, with a lower incidence of these pathologies being observed in young female mice when compared to age-matched males. Future investigations assessing insulin metabolism in female cKO mice would advance our understanding of the mechanisms underlying these sex-related changes in the susceptibility to diabetes and obesity.

Hormonally active osteocalcin (under- and uncarboxylated forms) acts to increase insulin secretion through β-cell proliferation and augments peripheral insulin sensitivity and energy expenditure (Ferron et al., 2010; Fulzele et al., 2010). We recently demonstrated that global *Enpp1*$^{-/-}$ mice have elevated levels of active osteocalcin and remain insulin sensitive following chronic HFD feeding (Huesa et al., 2014). Here we show that the insulin-resistant cKO mice also similarly exhibit increased concentrations of undercarboxylated and bioactive

osteocalcin. This suggests that osteocalcin regulation is a specific consequence of NPP1 in bone, with bone ENPP1 deficiency driving the increased plasma osteocalcin levels. These data support previous reports highlighting an osteocalcin-independent influence of osteoblasts on energy metabolism (Yoshikawa et al., 2011).

5 | CONCLUSION

Our data adds to the body of evidence supporting a role for ENPP1 in metabolic dysfunction. We demonstrate that osteoblast-specific ablation of NPP1 in mice alters osteocalcin carboxylation status whilst offering reduced protection against insulin resistance. Furthermore, future work assessing a wider range of bone phenotypes, including osteoclast function and comparison of appendicular to axial bones in these mice would be highly informative. A fuller understanding of the tissue-specific actions of ENPP1 is undoubtedly required to inform the development of new therapeutic strategies for treating diabetes.

Supplementary Material

Refer to Web version on PubMed Central for supplementary material.

ACKNOWLEDGMENTS

This study was supported by funding from the Biotechnology and Biological Sciences Research Council (BBSRC) in the form of an Institute Strategic Program Grant (BB/J004316/1; BBS/E/D/20221657) and International Partnering Award (BB/P02503X/1); British Heart Foundation (grant number PG/15/13/31296); pilot grant funding from Tenovus Scotland (E17/03) and R(D)VS PhD studentship funding.

Funding information

British Heart Foundation, Grant/Award Number: PG/15/13/31296; Tenovus Scotland, Grant/Award Number: E17/03; Biotechnology and Biological Sciences Research Council, Grant/Award Number: BB/J004316/1;BBS/E/D/20221657; BB/P02503X/1

DATA AVAILABILITY STATEMENT

The data that supports the findings of this study are available in the tables, main figures and supplementary material of this article.

REFERENCES

Anderson HC, Harmey D, Camacho NP, Garimella R, Sipe JB, Tague S, Bi X, Johnson K, Terkeltaub R, & Millán JL (2005). Sustained osteomalacia of long bones despite major improvement in other hypophosphatasia-related mineral deficits in tissue nonspecific alkaline phosphatase/nucleotide pyrophosphatase phosphodiesterase 1 double-deficient mice. American Journal of Pathology, 166(6), 1711–1720. 10.1016/s00029-440(10)62481-9 [PubMed: 15920156]

Babij P, Roudier M, Graves T, Han CYE, Chhoa M, Li CM, Juan T, Morony S, Grisanti M, Li X, Yu L, Dwyer D, Lloyd DJ, Bass MB, Richards WG, Ebeling C, Amato J, & Carlson G. (2009). New variants in the Enpp1 and Ptpn6 genes cause low BMD, crystal-related arthropathy, and vascular calcification. Journal of Bone and Mineral Research, 24(9), 1552–1564. 10.1359/jbmr.090417 [PubMed: 19419305]

BioGPS. (2018). Retrieved from http://biogps.org/#goto=genereport&id=5167

Bredella MA, Fazeli PK, Freedman LM, Calder G, Lee H, Rosen CJ, & Klibanski A. (2012). Young women with cold-activated brown adipose tissue have higher bone mineral density and lower Pref-1 than women without brown adipose tissue: A study in women with anorexia nervosa, women

recovered from anorexia nervosa, and normal-weight women. Journal of Clinical Endocrinology and Metabolism, 97(4), E584–E590. 10.1210/jc.2011-2246 [PubMed: 22259053]

Bredella MA, Gill CM, Rosen CJ, Klibanski A, & Torriani M. (2014). Positive effects of brown adipose tissue on femoral bone structure. Bone, 58, 55–58. 10.1016/j.bone.2013.10.007 [PubMed: 24140784]

Feldmann HM, Golozoubova V, Cannon B, & Nedergaard J. (2009). UCP1 ablation induces obesity and abolishes diet-induced thermogenesis in mice exempt from thermal stress by living at thermoneutrality. Cell Metabolism, 9(2), 203–209. 10.1016/j.cmet.2008.12.014 [PubMed: 19187776]

Ferron M, Wei J, Yoshizawa T, Ducy P, & Karsenty G. (2010). An ELISA-based method to quantify osteocalcin carboxylation in mice. Biochemical and Biophysical Research Communications, 397(4), 691–696. 10.1016/j.bbrc.2010.06.008 [PubMed: 20570657]

Fulzele K, Riddle RC, DiGirolamo DJ, Cao X, Wan C, Chen D, Faugere MC, Aja S, Hussain MA, Brüning JC, & Clemens TL (2010). Insulin receptor signaling in osteoblasts regulates postnatal bone acquisition and body composition. Cell, 142(2), 309–319. 10.1016/j.cell.2010.06.002 [PubMed: 20655471]

Goldfine ID, Maddux BA, Youngren JF, Reaven G, Accili D, Trischitta V, Vigneri R, & Frittitta L. (2008). The role of membrane glycoprotein plasma cell antigen 1/ectonucleotide pyrophosphatase phosphodiesterase 1 in the pathogenesis of insulin resistance and related abnormalities. Endocrine Reviews, 29(1), 62–75. 10.1210/er.2007-0004 [PubMed: 18199690]

Hajjawi M, Macrae V, Huesa C, Boyde A, Luis Millán J, Arnett T, & Orriss I. (2014). Mineralisation of collagen rich soft tissues and osteocyte lacunae in Enpp1(−/−) mice. Bone, 69, 139–147. [PubMed: 25260930]

Harmey D, Hessle L, Narisawa S, Johnson KA, Terkeltaub R, & Millán JL (2004). Concerted regulation of inorganic pyrophosphate and osteopontin by Akp2, Enpp1, and Ank: An integrated model of the pathogenesis of mineralization disorders. The American Journal of Pathology, 164(4), 1199–1209. 10.1016/S0002-9440(10)63208-7 [PubMed: 15039209]

Henderson NC, Arnold TD, Katamura Y, Giacomini MM, Rodriguez JD, McCarty JH, Pellicoro A, Raschperger E, Betsholtz C, Ruminski PG, Griggs DW, Prinsen MJ, Maher JJ, Iredale JP, Lacy-Hulbert A, Adams RH, & Sheppard D. (2013). Targeting of αv integrin identifies a core molecular pathway that regulates fibrosis in several organs. Nature Medicine, 19(12), 1617–1624. 10.1038/nm.3282

Hildebrand T, & Ruegsegger P. (1997). Quantification of bone microarchitecture with the structure model index. Computer Methods in Biomechanics and Biomedical Engineering, 1(1), 15–23. 10.1080/01495739708936692 [PubMed: 11264794]

Huesa C, Zhu D, Glover JD, Ferron M, Karsenty G, Milne EM, Millan JL, Ahmed SF, Farquharson C, Morton NM, & MacRae VE (2014). Deficiency of the bone mineralization inhibitor NPP1 protects mice against obesity and diabetes. Disease Models & Mechanisms, 7(12), 1341–1350. 10.1242/dmm.017905 [PubMed: 25368121]

Jansen RS, Duijst S, Mahakena S, Sommer D, Szeri F, Váradi A, Plomp A, Bergen AA, Oude Elferink RPJ, Borst P, & van de Wetering K. (2014). ABCC6-mediated ATP secretion by the liver is the main source of the mineralization inhibitor inorganic pyrophosphate in the systemic circulation-brief report. Arteriosclerosis, Thrombosis, and Vascular Biology, 34(9), 1985–1989. 10.1161/ATVBAHA.114.304017 [PubMed: 24969777]

Jansen RS, Kucukosmanoglu A, de Haas M, Sapthu S, Otero JA, Hegman IEM, Bergen AAB, Gorgels TGMF, Borst P, & van de Wetering K. (2013). ABCC6 prevents ectopic mineralization seen in pseudoxanthoma elasticum by inducing cellular nucleotide release. Proceedings of the National Academy of Sciences, 110(50), 20206–20211. 10.1073/pnas.1319582110

Johnson K, Goding J, Van Etten D, Sali A, Hu SI, Farley D, Krug H, Hessle L, Millán JL, & Terkeltaub R. (2003). Linked deficiencies in extracellular PP(i) and osteopontin mediate pathologic calcification associated with defective PC-1 and ANK expression. Journal of Bone and Mineral Research, 18(6), 994–1004. 10.1359/jbmr.2003.18.6.994 [PubMed: 12817751]

Johnson K, Pritzker K, Goding J, & Terkeltaub R. (2001). The nucleoside triphosphate pyrophosphohydrolase isozyme PC-1 directly promotes cartilage calcification through chondrocyte

apoptosis and increased calcium precipitation by mineralizing vesicles. The Journal of Rheumatology, 28(12), 2681. [PubMed: 11764218]

Karsenty G, Ferron M, Karsenty G, & Ferron M. (2012). The contribution of bone to whole-organism physiology. Nature, 481, 314–320. [PubMed: 22258610]

Karsenty G, & Olson EN (2016). Bone and muscle endocrine functions: Unexpected paradigms of inter-organ communication. Cell, 164(6), 1248–1256. 10.1016/j.cell.2016.02.043 [PubMed: 26967290]

Kim S.ooM., Lun M, Wang M, Senyo S, Guillermier C, Patwari P, & Steinhauser M.atthewL. (2014). Loss of white adipose hyperplastic potential is associated with enhanced susceptibility to insulin resistance. Cell Metabolism, 20(6), 1049–1058. 10.1016/j.cmet.2014.10.010 [PubMed: 25456741]

Lee P, Brychta RJ, Collins MT, Linderman J, Smith S, Herscovitch P, Millo C, Chen KY, & Celi FS (2013). Cold-activated brown adipose tissue is an independent predictor of higher bone mineral density in women. Osteoporosis International, 24(4), 1513–1518. 10.1007/s00198-012-2110-y [PubMed: 22890364]

Lee Kim, H. E., Bae SJ, Choe J, Jung CH, Lee WJ, & Kim HK (2019). Protective role of skeletal muscle mass against progression from metabolically healthy to unhealthy phenotype. Clin Endocrinol, 90(1), 102–113. 10.1111/cen.13874

Li Q, Guo H, Chou DW, Berndt A, Sundberg JP, & Uitto J. (2013). Mutant Enpp1asj mice as a model for generalized arterial calcification of infancy. Disease Models & Mechanisms, 6(5), 1227–1235. 10.1242/dmm.012765 [PubMed: 23798568]

Lim S, Honek J, Xue Y, Seki T, Cao Z, Andersson P, Yang X, Hosaka K, & Cao Y. (2012). Cold-induced activation of brown adipose tissue and adipose angiogenesis in mice. Nature Protocols, 7(3), 606–615. 10.1038/nprot.2012.013 [PubMed: 22383039]

Mackenzie NCW, Zhu D, Milne EM, van 't Hof R, Martin A, Quarles DL, Millán JL, Farquharson C, & MacRae VE (2012). Altered bone development and an increase in FGF-23 expression in Enpp1−/− mice. PLOS One, 7(2), e32177. 10.1371/journal.pone.0032177

Millán JL (2013). The role of phosphatases in the initiation of skeletal mineralization. Calcified Tissue International, 93(4), 299–306. 10.1007/s00223-012-9672-8 [PubMed: 23183786]

Nedergaard J, & Cannon B. (2010). The changed metabolic world with human brown adipose tissue: Therapeutic visions. Cell Metabolism, 11(4), 268–272. 10.1016/j.cmet.2010.03.007 [PubMed: 20374959]

Prudente S, Morini E, & Trischitta V. (2009). Insulin signaling regulating genes: Effect on T2DM and cardiovascular risk. Nature Reviews Endocrinology, 5(12), 682–693. 10.1038/nrendo.2009.215

Roberts F, Zhu D, Farquharson C, & Macrae V. (2019). ENPP1 in the regulation of mineralization and beyond. Trends in Biochemical Sciences, 10.1016/j.tibs.2019.01.010

Rueden CT, Schindelin J, Hiner MC, DeZonia BE, Walter AE, Arena ET, & Eliceiri KW (2017). ImageJ2: ImageJ for the next generation of scientific image data. BMC Bioinformatics, 18(1), 529. 10.1186/s12859-017-1934-z [PubMed: 29187165]

St Hilaire C, Ziegler SG, Markello TC, Brusco A, Groden C, Gill F, Carlson-Donohoe H, Lederman RJ, Chen MY, Yang D, Siegenthaler MP, Arduino C, Mancini C, Freudenthal B, Stanescu HC, Zdebik AA, Chaganti RK, Nussbaum RL, Kleta R, … Boehm M. (2011). NT5E mutations and arterial calcifications. New England Journal of Medicine, 364(5), 432–442. 10.1056/NEJMoa0912923 [PubMed: 21288095]

Staines KA, Javaheri B, Hohenstein P, Fleming R, Ikpegbu E, Unger E, Hopkinson M, Buttle DJ, Pitsillides AA, & Farquharson C. (2017). Hypomorphic conditional deletion of E11/Podoplanin reveals a role in osteocyte dendrite elongation. Journal of Cellular Physiology, 232(11), 3006–3019. 10.1002/jcp.25999 [PubMed: 28488815]

Terkeltaub R. (2006). Physiologic and pathologic functions of the NPP nucleotide pyrophosphatase/phosphodiesterase family focusing on NPP1 in calcification. Purinergic signalling, 2(2), 371–377. 10.1007/s11302-005-5304-3 [PubMed: 18404477]

Xue Y, Petrovic N, Cao R, Larsson O, Lim S, Chen S, Feldmann HM, Liang Z, Zhu Z, Nedergaard J, Cannon B, & Cao Y. (2009). Hypoxia-independent angiogenesis in adipose tissues during cold acclimation. Cell Metabolism, 9(1), 99–109. 10.1016/j.cmet.2008.11.009 [PubMed: 19117550]

Yoshikawa Y, Kode A, Xu L, Mosialou I, Silva BC, Ferron M, Clemens TL, Economides AN, & Kousteni S. (2011). Genetic evidence points to an osteocalcin-independent influence of osteoblasts on energy metabolism. Journal of Bone and Mineral Research, 26(9), 2012–2025. 10.1002/jbmr.417 [PubMed: 21557308]

Zhang M, Xuan S, Bouxsein ML, von Stechow D, Akeno N, Faugere MC, Malluche H, Zhao G, Rosen CJ, Efstratiadis A, & Clemens TL (2002). Osteoblast-specific knockout of the insulin-like growth factor (IGF) receptor gene reveals an essential role of IGF signaling in bone matrix mineralization. Journal of Biological Chemistry, 277(46), 44005–44012. 10.1074/jbc.M208265200 [PubMed: 12215457]

Zhao J, Kingman J, Sundberg JP, Uitto J, & Li Q. (2017). Plasma PPi deficiency Is the major, but not the exclusive, cause of ectopic mineralization in an Abcc6(−/−) mouse model of PXE. Journal of Investigative Dermatology, 137(11), 2336–2343. 10.1016/j.jid.2017.06.006 [PubMed: 28652107]

Zhu D, Mackenzie NCW, Millan JL, Farquharson C, & MacRae VE (2013). A protective role for FGF-23 in local defence against disrupted arterial wall integrity? Molecular and Cellular Endocrinology, 372(1-2), 1–11. 10.1016/j.mce.2013.03.008 [PubMed: 23523568]

Zhu D, Mackenzie NCW, Millán JL, Farquharson C, & MacRae VE (2011). The appearance and modulation of osteocyte marker expression during calcification of vascular smooth muscle cells. PLOS One, 6(5), e19595. 10.1371/journal.pone.0019595

Zhu D, Mackenzie NCW, Shanahan CM, Shroff RC, Farquharson C, & MacRae VE (2015). BMP-9 regulates the osteoblastic differentiation and calcification of vascular smooth muscle cells through an ALK1 mediated pathway. Journal of Cellular and Molecular Medicine, 19(1), 165–174. 10.1111/jcmm.12373 [PubMed: 25297851]

Ziegler SG, Ferreira CR, MacFarlane EG, Riddle RC, Tomlinson RE, Chew EY, Martin L, Ma CT, Sergienko E, Pinkerton AB, Millán JL, Gahl WA, & Dietz HC (2017). Ectopic calcification in pseudoxanthoma elasticum responds to inhibition of tissue-nonspecific alkaline phosphatase. Science Translational Medicine, 9(393), eaal1669. 10.1126/scitranslmed.aal1669

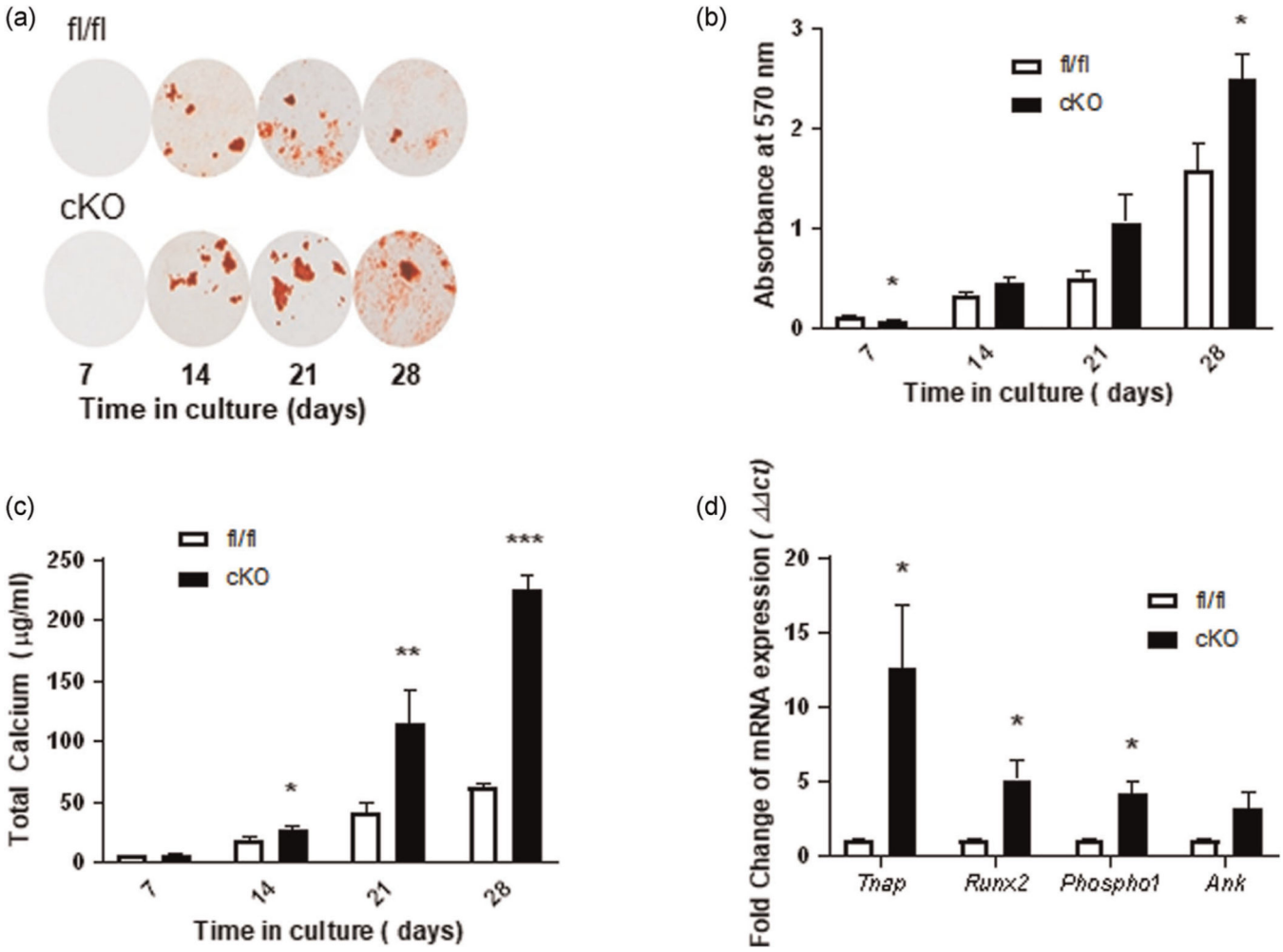

FIGURE 1.

The matrix of *Enpp1* deficient calvariae osteoblasts show a hypermineralized phenotype in vitro. (a) Representative image of alizarin red stained primary osteoblast cells, (b) quantification of alizarin red stain, (c) quantification of total calcium, and (D) Rrelative mRNA expression of osteogenic and mineralization markers including *Tnap*, *Runx2*, *Phospho1*, and *Ank* at Day 0. Data are presented as the mean ± *SEM* ($n = 6$). Significance is denoted by $*p < .05$, $**p < .01$, and $***p < .001$. cKO, conditional knockout mice; mRNA, messenger RNA

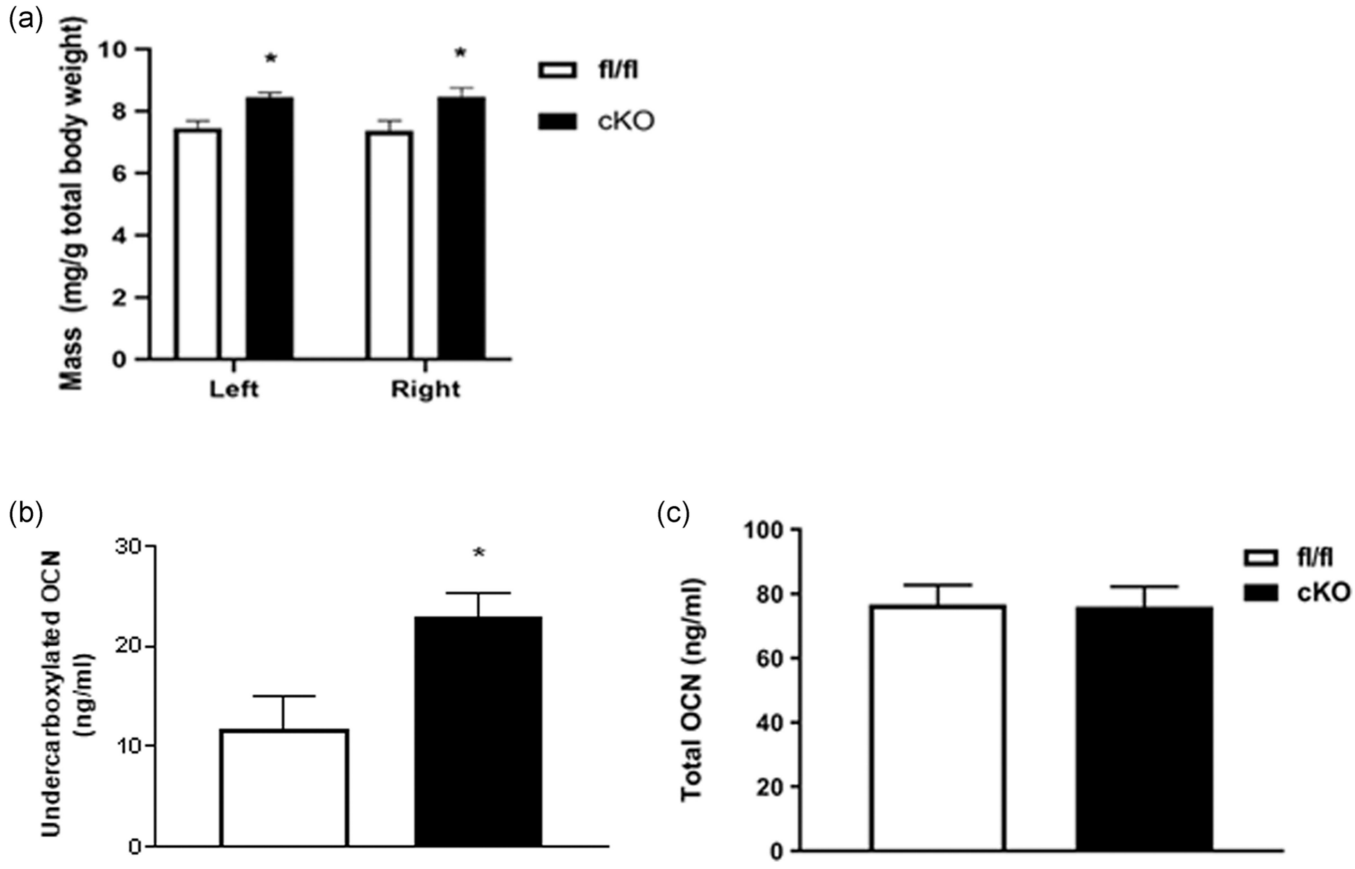

FIGURE 2.

cKO mice display an altered *quadriceps femoris* mass and osteocalcin levels. (a) Muscle mass of male cKO and *fl/fl* mice at 16-weeks of age ($n = 6$). (b) Undercarboxylated osteocalcin (OCN) levels and (c) total OCN levels in 16-week-old male *fl/fl* and cKO mice ($n = 6$). Data are presented as the mean ± *SEM*. Significance is denoted by $*p < .05$. cKP, conditional knockout mice

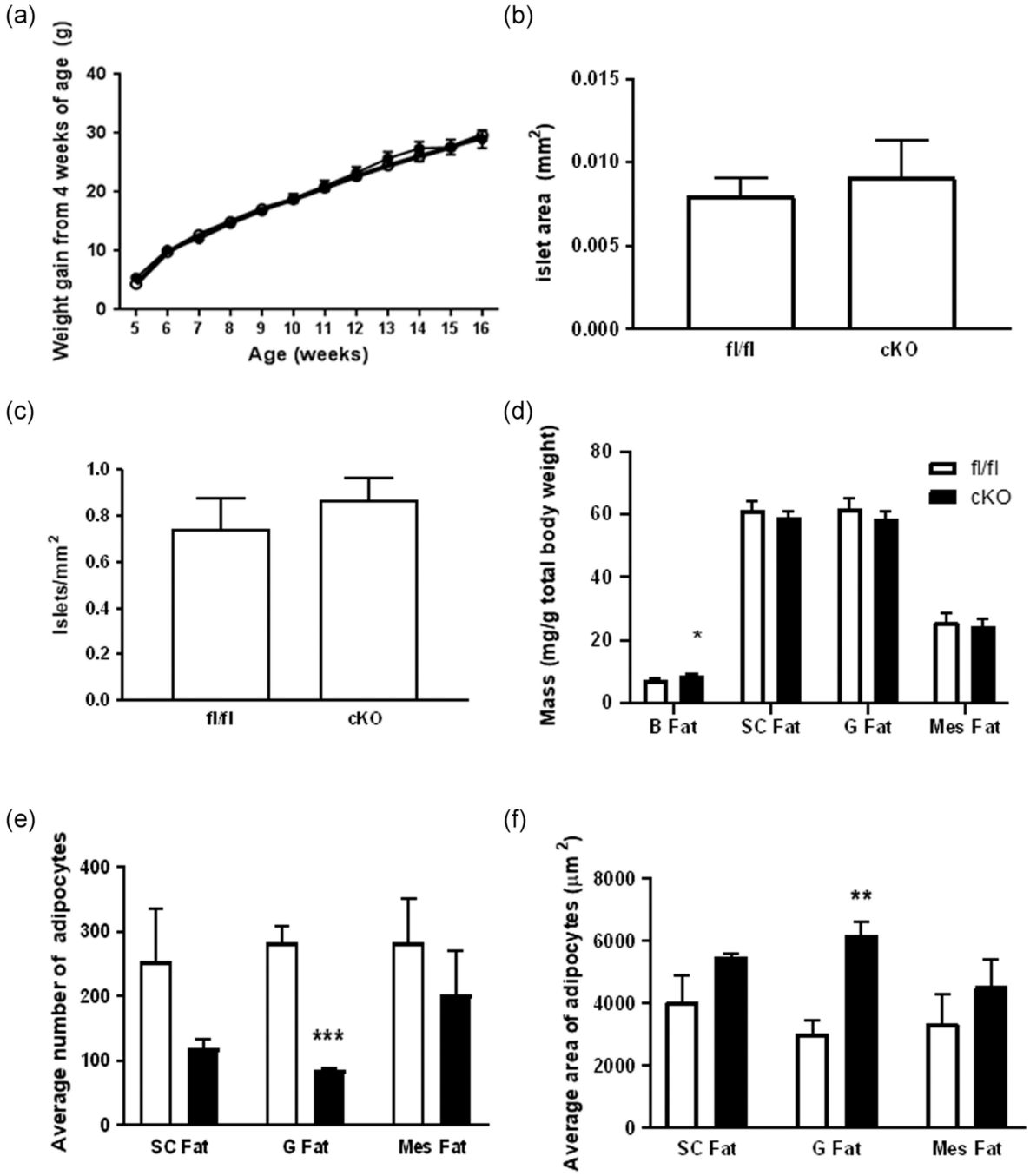

FIGURE 3.

Assessment of pancreatic and fat tissue morphology in cKO and *fl/fl* male mice following a chronic high-fat diet (HFD) challenge. (a) Weekly weight gain of HFD challenged cKO and *fl/fl* mice ($n \geq 7$). (b) Pancreatic islet area and (c) Islet number ($n \geq 4$). (d) Average mass of brown (B), sub-cutaneous (SC), gonadal (G), and mesenteric (Mes) fat ($n \geq 4$). The average (e) number and (f) area of adipocytes in SC, G, and Mes fat ($n \geq 4$) of HFD challenged cKO and *fl/fl* mice at 16 weeks of age. Data are presented as the mean ± *SEM*. Significance is denoted by $*p < .05$, $**p < .01$, and $***p < .001$. cKO, conditional knockout mice

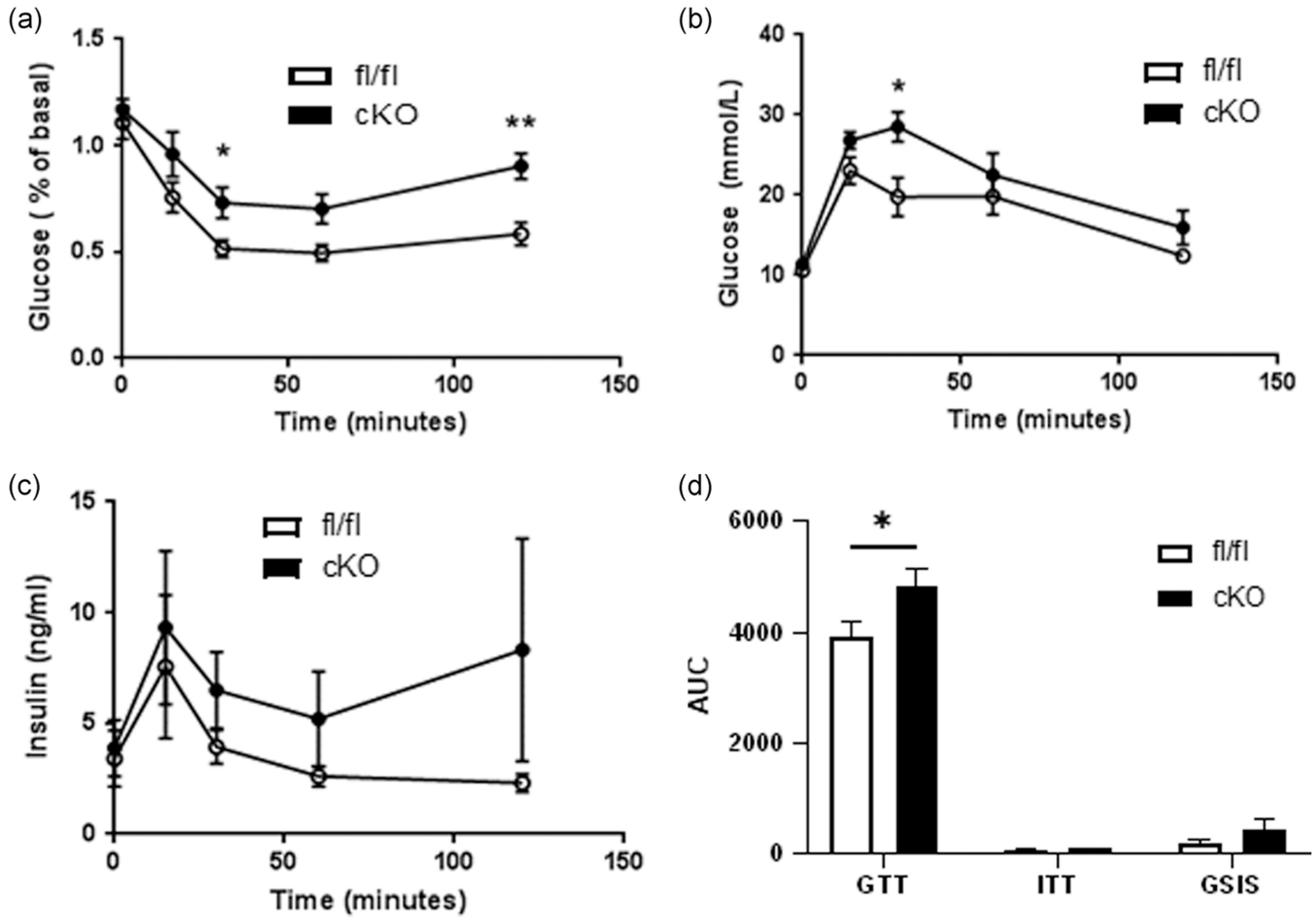

FIGURE 4.

cKO mice show increased insulin resistance in response to a chronic HFD challenge. (a) Insulin tolerance test, (b) glucose tolerance test, and (c) glucose stimulated insulin secretion. (d) Metabolic tests analyzed as area under the curve. Mice were reared under high-fat dietary conditions and were 16-weeks of age. Data are presented as the mean ± *SEM* ($n \geq 6$). Significance is denoted by *$p < .05$, **$p < .01$, and ***$p < .001$. AUC, area under the curve; cKO, conditional knockout mice; HFD, high-fat diet

TABLE 1

Micro-CT analysis of the femur and tibia cortical bone from 6-week-old male and female cKO and *fl/fl* mice

Bone	Gender	Genotype	Peri. Di (mm)	Endo. Di (mm)	BV (mm^3)	Tb. Th (mm)	Po(op) (%)
Femur	Male	*fl/fl*	2.144 (0.06)	1.773 (0.06)	0.800 (0.05)	0.117 (0.00)	2.059 (0.30)
		cKO	2.147 (0.04)	1.783 (0.06)	0.815 (0.02)	0.109 (0.00)*	2.828 (0.19)
	Female	*fl/fl*	1.97 (0.03)	1.67 (0.03)	0.565 (0.03)	0.106 (0.02)	2.04 (0.09)
		cKO	2.25 (0.03)	1.95 (0.03)***	0.64 (0.04)	0.100 (0.03)	2.46 (0.14)*
Tibia	Male	*fl/fl*	1.66 (0.05)*	1.277 (0.07)	0.857 (0.04)	0.101 (0.01)	3.467 (0.50)
		cKO	1.817 (0.02)	1.357 (0.03)	0.859 (0.02)	0.09 (0.00)	4.128 (0.29)
	Female	*fl/fl*	1.57 (0.13)	1.29 (0.02)	0.624 (0.02)	0.09 (0.02)	3.35 (0.28)
		cKO	1.89 (0.04)*	1.48 (0.03)***	0.68 (0.03)	0.08 (0.03)	3.53 (0.16)

Note: Data presented as the mean ± *SEM* ($n \geq 4$).

Abbreviations: BV, bone volume; cKO, conditional knockout mice; CT, computed tomography.

* $p < .05$.

*** $p < .001$.

TABLE 2

Micro-CT analysis of the femur and tibia trabecular parameters of 6-week-old male and female cKO and *fl/fl* mice

Bone	Gender	Genotype	BV/TV %	BMD (g/cm^3)	Tb. Pf	Tb. Th (μm)	Tb. No	Tb. Sp (mm)	SMI
Femur	Male	*fl/fl*	22.40 (1.98)	0.31 (0.02)	7.24 (3.04)	41.1 (0.00)	5.24 (0.34)	0.14 (0.11)	1.05 (0.55)
		cKO	26.96 (5.88)	0.30 (0.03)	4.15 (2.80)	44.38 (0.00)	6.023 (0.26)	0.13 (0.03)	0.928 (0.31)
	Female	*fl/fl*	11.99 (0.65)	0.32 (0.01)	23.22 (1.48)	36.37 (0.00)	3.29 (0.13)	0.19 (0.00)	1.668 (0.05)
		cKO	17.50 (0.58)***	0.36 (0.02)	15.29 (1.42)**	38.06 (0.00)	4.61 (0.15)***	0.18 (0.00)	1.39 (0.05)**
Tibia	Male	*fl/fl*	16.60 (1.55)	0.246 (0.01)	22.43 (2.50)	39.80 (0.00)	4.12 (0.26)	0.14 (0.01)	1.77 (0.09)
		cKO	16.68 (0.94)	0.26 (0.02)	21.59 (1.93)	40.15 (0.00)	4.12 (0.15)	0.15 (0.00)	1.71 (0.05)
	Female	*fl/fl*	7.675 (0.57)	0.16 (0.01)*	34.79 (2.70)	34.18 (0.09)	2.24 (0.16)	0.22 (0.01)	2.03 (0.09)
		cKO	10.92 (0.72)**	0.198 (0.01)	29.76 (3.38)	33.62 (0.00)	3.23 (0.12)***	0.18 (0.01)***	1.85 (0.06)

Note: Data presented as the mean ± *SEM* ($n \geq 5$). Significance is denoted by *$p < .05$, **$p < .01$, ***$p < .001$.

Abbreviations: BV/TV, bone volume fraction; cKO, conditional knockout mice; CT, computed tomography; SMI, structure model index.

*$p < .05$.

**$p < .01$.

***$p < .001$.